Received: 17 July 2019 | Revised: 2 November 2019 | Accepted: 21 November 2019

DOI: 10.1111/jnc.14928

ORIGINAL ARTICLE

Journal of Neurochemistry JNC The Official Journal of the International Society for Neurochemistry WILEY

Enteric short-chain fatty acids promote proliferation of human neural progenitor cells

Liu L. Yang[1,2] | Vincent Millischer[1,2] | Sergey Rodin[3] | Derrick F. MacFabe[4,5] | Juan C. Villaescusa[1,2] | Catharina Lavebratt[1,2]

[1]Department of Molecular Medicine and Surgery, Karolinska Institute, Stockholm, Sweden

[2]Center for Molecular Medicine, Karolinska University Hospital Solna, Stockholm, Sweden

[3]Division of Matrix Biology, Department of Medical Biochemistry and Biophysics, Karolinska Institute, Stockholm, Sweden

[4]The Kilee Patchell-Evans Autism Research Group, London, Canada

[5]Center for Healthy Eating and Food Innovation, Faculty of Medicine, Maastricht University, Maastricht, Netherlands

Correspondence
Catharina Lavebratt, Center for molecular medicine, Karolinska University Hospital Solna, Stockholm.
Email: catharina.lavebratt@ki.se

Funding information
Swedish Research Council; Brain Foundation; China Scholarship Council

Abstract

Short-chain fatty acids (SCFAs) are a group of fatty acids predominantly produced during the fermentation of dietary fibers by the gut anaerobic microbiota. SCFAs affect many host processes in health and disease. SCFAs play an important role in the 'gut-brain axis', regulating central nervous system processes, for example, cell–cell interaction, neurotransmitter synthesis and release, microglia activation, mitochondrial function, and gene expression. SCFAs also promote the growth of neurospheres from human neural stem cells and the differentiation of embryonic stem cells into neural cells. It is plausible that maternally derived SCFAs may pass the placenta and expose the fetus at key developmental periods. However, it is unclear how SCFA exposure at physiological levels influence the early-stage neural cells. In this study, we explored the effect of SCFAs on the growth rate of human neural progenitor cells (hNPCs), generated from human embryonic stem cell line (HS980), with IncuCyte live-cell analysis system and immunofluorescence. We found that physiologically relevant levels (μM) of SCFAs (acetate, propionate, butyrate) increased the growth rate of hNPCs significantly and induced more cells to undergo mitosis, while high levels (mM) of SCFAs had toxic effects on hNPCs. Moreover, no effect on apoptosis was observed in physiological-dose SCFA treatments. In support, data from q-RT PCR showed that SCFA treatments influenced the expression of the neurogenesis, proliferation, and apoptosis-related genes *ATR*, *BCL2*, *BID*, *CASP8*, *CDK2*, *E2F1*, *FAS*, *NDN*, and *VEGFA*. To conclude, our results propose that SCFAs regulates early neural system development. This might be relevant for a putative 'maternal gut-fetal brain-axis'.

KEYWORDS

gut microbiota, human neural progenitor cells, neurodevelopment, proliferation, short-chain fatty acids

Abbreviations used: *ADORA1*, adenosine A1 receptor; *ADORA2A*, adenosine A2a receptor; ASD, autism spectrum disorder; *ATCB*, β-actin; *ATR*, serine/threonine kinase; BBB, blood–brain barrier; *BCL2*, BCL2 apoptosis regulator; *BID*, BH3-interacting domain death agonist; *CASP3*, caspase 3; *CASP8*, caspase 8; *CCND2*, cyclin D2; *CDK1*, cyclin-dependent kinase 1; *CDK2*, cyclin-dependent kinase 2; CNS, central nerve system; CSF, cerebrospinal fluid; *E2F1*, E2F transcription factor 1; *EP300*, E1A-binding protein P300; *FAS*, fas cell surface death receptor; *GAPDH*, glyceraldehyde-3-phosphate dehydrogenase; GI, gastrointestinal; GPR 41/43, G-protein-coupled receptor 41/43; HDAC, histone deacetylase; *HDAC4*, histone deacetylase 4; hNPCs, human neural progenitor cells; hNSCs, human neural stem cells; IQR, interquartile range; *NDN*, necdin; *NOTCH2*, notch receptor 2; PBS, phosphate-buffered saline; pHH3, phospho-histone H3; PI, propidium iodide; qRT-PCR, quantitative reverse transcriptase PCR; RRID, research resource identifier; SCFAs, short-chain fatty acids; *TP53*, tumor protein P53; *VEGFA*, vascular endothelial growth factor A.

1 | INTRODUCTION

1.1 | Gut microbiota and gut–brain axis

The human body harbors an ecosystem of gut microbiota that is dynamic throughout the lifespan. In rodent models, there is strong evidence that the gut bacterial microbiota can cause behavioral changes (Ntranos & Casaccia, 2018; Luczynski et al. 2016). Transferring feces from patients diagnosed with autism, depression, or schizophrenia to the rodent intestine produced behaviors and biochemical modulations related to these disorders (Kelly, Borre, & C, O. B., 2016; Sharon, Cruz, & Kang, 2019; Zheng, Zeng, & Liu, 2019). The gut microbiota plays a major role in the bidirectional communication between the GI tract and the central nervous system, the so-called gut–brain axis. This communication is mediated by neural pathways (e.g., the vagus nerve), immune activation, hormones (e.g., the hypothalamic–pituitary–adrenal axis), and metabolites (e.g., tryptophan and short-chain fatty acids (SCFAs)) produced by gut microbiota (Bienenstock, Kunze, & Forsythe, 2015). By studying germ-free and antibiotic drug-treated rodents, the SCFAs and the vagus nerve have been proposed to be key gut–brain axis mediators (Dinan & Cryan, 2017; MacFabe, 2015).

1.2 | SCFAs

SCFAs are fatty acids with 2–5 carbon atoms, of which acetate (C2), propionate (C3), and butyrate (C4) are the most abundant. They are the predominant metabolites that arise from the fermentation of dietary fibers, such as resistant starch, by anaerobic colonic microbiota, but are also present naturally or as an additive in diet (Cummings, Pomare, Branch, Naylor, & Macfarlane, 1987; Kasubuchi, Hasegawa, Hiramatsu, Ichimura, & Kimura, 2015; MacFabe, 2015). SCFAs are an essential energy source for intestinal cells (Hu, Lin, Zheng, & Cheung, 2018), strengthen the gut barrier function and have immune-modulatory effects in the intestine, exerting anti-carcinogenic and anti-inflammatory properties (Sivaprakasam, Prasad, & Singh, 2016). SCFAs are soluble in both water and lipids and they can be absorbed through passive diffusion, but their cellular uptake is enhanced by monocarboxylate transporters (Vijay & Morris, 2014). Dietary SCFAs as well as those produced by bacteria in the oral cavity, esophagus, distal colon, rectum, and epidermis may escape hepatic clearance and thereby get systemic access (MacFabe, 2015) and then pass the blood–brain barrier (BBB) (Tsuji, 2005). G-protein-coupled receptors (GPR41, GPR43), named also free fatty acid receptors (FFAR3, FFAR2), were the main receptors that found to be activated by all the three SCFAs (Kasubuchi et al., 2015; Miyamoto et al., 2016). GPR41/43 are known to be expressed on a wide range of cell types, including the human intestinal epithelial cells, adipose cells, immune cells, pancreatic β cells, brain endothelium, and neural cells in ganglia (Miyamoto et al., 2016).

The metabolism of SCFAs is complex. However, the SCFAs have been suggested to have broad influences on the physiology of the nervous system including calcium-dependent neurotransmitter release (rats) (DeCastro et al., 2005; Severson, Wang, Pieribone, Dohle, & Richerson, 2003), electrophysiology, neuroinflammation, lipid metabolism (rats) (MacFabe, 2015), closure of gap junctions, intracellular acidification (rats) (Rorig, Klausa, & Sutor, 1996), microglial maturation and activation (mice) (Erny, Hrabe de Angelis, & Jaitin, 2015), as well as mitochondrial function and oxidative stress (animals and human) (Frye, Melnyk, & Macfabe, 2013; Hecker, Sommer, & Voigtmann, 2014). SCFAs influence gap junction gating also in the BBB, and are hence essential for a functioning BBB in mice (Braniste, Al-Asmakh, & Kowal, 2014; Hoyles et al., 2018). Some of these effects are likely mediated by the SCFA receptors (GPR41/GPR43). Other SCFA effects, especially of propionate and butyrate, are mediated through their histone deacetylase (HDAC) inhibitory activity, which results in epigenetically regulated gene expression (Nankova, Agarwal, MacFabe, & Gamma, 2014; Patnala, Arumugam, Gupta, & Dheen, 2017). Furthermore, sodium butyrate was shown to stimulate brain-derived neurotrophic factor expression, neurogenesis, and neural proliferation in rodents (Kim, Leeds, & Chuang, 2009; Wei, Melas, Wegener, Mathe, & Lavebratt, 2014; Yoo et al., 2011) and to facilitate long-term memory consolidation (Levenson et al., 2004). Emerging evidence shows that species-rich enteric microbiota and metabolites, such as propionate, play a major role in normal brain and behavioral development (Diaz Heijtz et al., 2011; Hsiao, McBride, & Hsien, 2013) and are altered in neurodevelopmental disorder like autism (MacFabe, 2015).

Most in vitro studies of SCFAs investigated their effects on cancer cells, such as colorectal cancer cells (Van Rymenant et al., 2017), breast cancer cells (Wang et al., 2016), non-small-cell lung carcinoma cells (Jin, Wu, Dai, Li, & Xiao, 2017), osteosarcoma cells (Perego, Sansoni, Banfi, & Lombardi, 2018) and other cells like adipocytes (Hu, Kyrou, & Tan, 2016) and immune cells (Patnala et al., 2017). So far, however, only few studies have been performed on the effects of SCFAs on human early neural cells. A study from Yao et al. reported that sodium butyrate promoted the differentiation of mouse embryonic stem cells into neural cells (Yao et al., 2010). Moreover the concentrations of SCFAs applied in these studies (in the mM range) have been much higher than the reported physiological levels (μM range), but for in a recent in vitro study on a human BBB cell model that was conducted using a physiologically relevant propionate concentration at 1 μM (Hoyles et al., 2018). As previously mentioned, we have examined metabolic, immunological, and epigenetic effects in rodent PC12 cells, and lymphoblasts from neurotypical and autistic patients (Frye et al., 2017; Nankova et al., 2014; Rose, Bennuri, & Davis, 2018). The detectable physiological levels of acetate, propionate, and butyrate differ between types of human body fluid, but are typically in the range of (acetate 0–410 μM; propionate 0–18.3 μM; butyrate 0–81 μM), including blood, cerebrospinal fluid (CSF), breast milk, and urine (Human Metabolome Database, http://www.hmdb.ca/). The relative levels of the three SCFAs corresponds to approximately 30:2:1 for acetate: propionate: butyrate (De Baere et al., 2013; Nagashima et al., 2010; Zhao et al., 2017).

1.3 | Effects of SCFAs on the fetus

In mice, maternal diet and microbiota reversibly affect the social behaviors and synaptic activity in offspring (Buffington et al., 2016). Subcutaneous injection of propionate into pregnant dams increased the anxious and antisocial behavior in female rat offspring (Foley, Ossenkopp, Kavaliers, & Macfabe, 2014; MacFabe, 2015). Prenatal maternal exposure to propionic acids associated with autism spectrum disorder development and produced similar biochemical effects in animal models and cell lines (Foley et al., 2014; MacFabe, 2015; Nankova et al., 2014). Other reported effects on fetuses of maternal dietary SCFA supplementation include increased number of fetuses and decreased abortion rate in mice (Lin et al., 2014). Non-interventional prenatal exposure to SCFAs is thought to primarily be gut-produced SCFAs in the maternal blood passing over the placenta to the fetus. However, the fetus is exposed to SCFAs present also in the amniotic fluid (Orczyk-Pawilowicz et al., 2016). Live microbes, including those capable of producing SCFA, or microbial DNA were found in human amniotic fluid (Stinson, Boyce, Payne, & Keelan, 2019), placenta (Aagaard et al., 2014), meconium (Ardissone, Cruz, & Davis-Richardson, 2014), as well as umbilical cord blood (Jimenez, Fernandez, & Marin, 2005). Taken together, there is a possibility that the SCFAs in the maternal blood, produced by the maternal intestinal or amniotic microbiota, expose the fetus and influence the fetal neurodevelopment. The aim of this study was to explore if SCFAs affect the growth of early stage neural cells, using human neural progenitor cells (hNPCs) as an in vitro model.

2 | MATERIALS AND METHODS

All reagents in this study were purchased within 2 years and stored properly according to the manufacturer's instructions. All experiments were performed and repeated according to the same time schedule during February 2018 to October 2019.

2.1 | CULTIVATION OF HUMAN EMBRYONIC STEM CELLS

Human embryonic stem cell line HS980 (RRID: CVCL_2Z88) (Rodin, Antonsson, & Niaudet, 2014) was provided by Professor Outi Hovatta (Karolinska Institutet). Cultivation and in vitro experimentation of this cell line was approved by the Swedish ethical review board in Stockholm (2017/1079-31/1). The study was not pre-registered. Cells were cultured in NutriStem hESC XF medium (cat. #05-100-1A, Biological Industries, Israel) on laminin-521 (LN-521, 30 μg/ml, cat. #LN-521, BioLamina, Stockholm, Sweden), in a similar way as described previously (Rodin et al., 2014). Cells were passaged by exposure to TrypLE Select (cat. #12563011, Gibco, New York, USA) for 4–5 min at 37°C, 5% CO_2. Before detaching, the enzyme was carefully aspirated and pre-warmed NutriStem medium was added to carefully wash the cells. After that, the cells were gently detached with 1 ml of pre-warmed NutriStem medium by pipetting into single-cell suspension and a desired fraction of cells was plated on a fresh LN-521-coated dish.

2.2 | GENERATION OF HUMAN NEURAL PROGENITOR CELLS (HNPCS)

hNPCs were generated from the human embryonic stem cell line (HS980) (Rodin et al., 2014) as described previously (Falk, Koch, & Kesavan, 2012; Koch, Opitz, Steinbeck, Ladewig, & Brustle, 2009). Briefly, cells were dissociated into single cells using TrypLE Select and plated on non-adhesive plastic in DMEM/F12 (cat. #31331028, Gibco) supplemented with 1% N2 (cat. #17502001, Gibco), SMAD inhibitors, SB-431542 (cat. #S4317, Sigma-Aldrich) and LDN-193189 (cat. #SML0559, Sigma-Aldrich). 50% of the media was changed every day, and 6-day-old floating aggregates were plated on tissue culture plates coated with 0.002% poly-L-ornithine (cat. #P4957, Sigma-Aldrich) and 20 μg/ml murine laminin (cat. #L2020, Sigma-Aldrich). Neural rosette structures started to emerge 2–3 days after plating. Neural rosettes were manually selected at day 4 and transferred to a new coated well in high density in DMEM/F12 media supplemented with 10 ng/ml FGF2, 10 ng/ml EGF (cat. #01-A01110 and #01-AA060, both from ORF Genetics, Kopavogur, Iceland), 1% N2 and 0.1% B27 (cat. #17504044, Gibco). The HS980 cell line could be maintained and expanded in the same media to at least 45 passages at our laboratory and the generated hNPCs were cultured from passage 0 to 25 at our laboratory (Figure 1a and Figure S1).

2.3 | SCFA EXPOSURE ON HNPCS

The concentrations of SCFAs for our in vitro experiments were selected for two sub-studies (Table 1A and B). First, for the toxicity test, concentrations ranging from 1 μM to 192 mM were selected based on the current in vitro literature (mM) and the relative levels in human body fluid (acetate: propionate: butyrate ≈ 30:2:1). Second, for the experimental test of physiologically relevant SCFA levels, concentrations were selected based on the previously reported levels in human body fluid that did not have toxic effects in our in vitro toxicity test (concentrations lower than T3, Table 1B). The reported levels of the three SCFAs in CSF of healthy population are: acetate: 31–410 μM, propionate 0–6 μM, butyrate 0–2.8 μM (Human Metabolome Database, http://www.hmdb.ca/). Sodium acetate (cat. #71196, Sigma-Aldrich), sodium propionate (cat. #P5436, Sigma-Aldrich) and sodium butyrate (cat. #TR-1008-G, Merck Millipore) and water as control were added (1:100 dilution in cell culture medium) to obtain the listed concentrations, immediately after splitting cells from a six-well plate into a 48-well plate (Figure 1b).

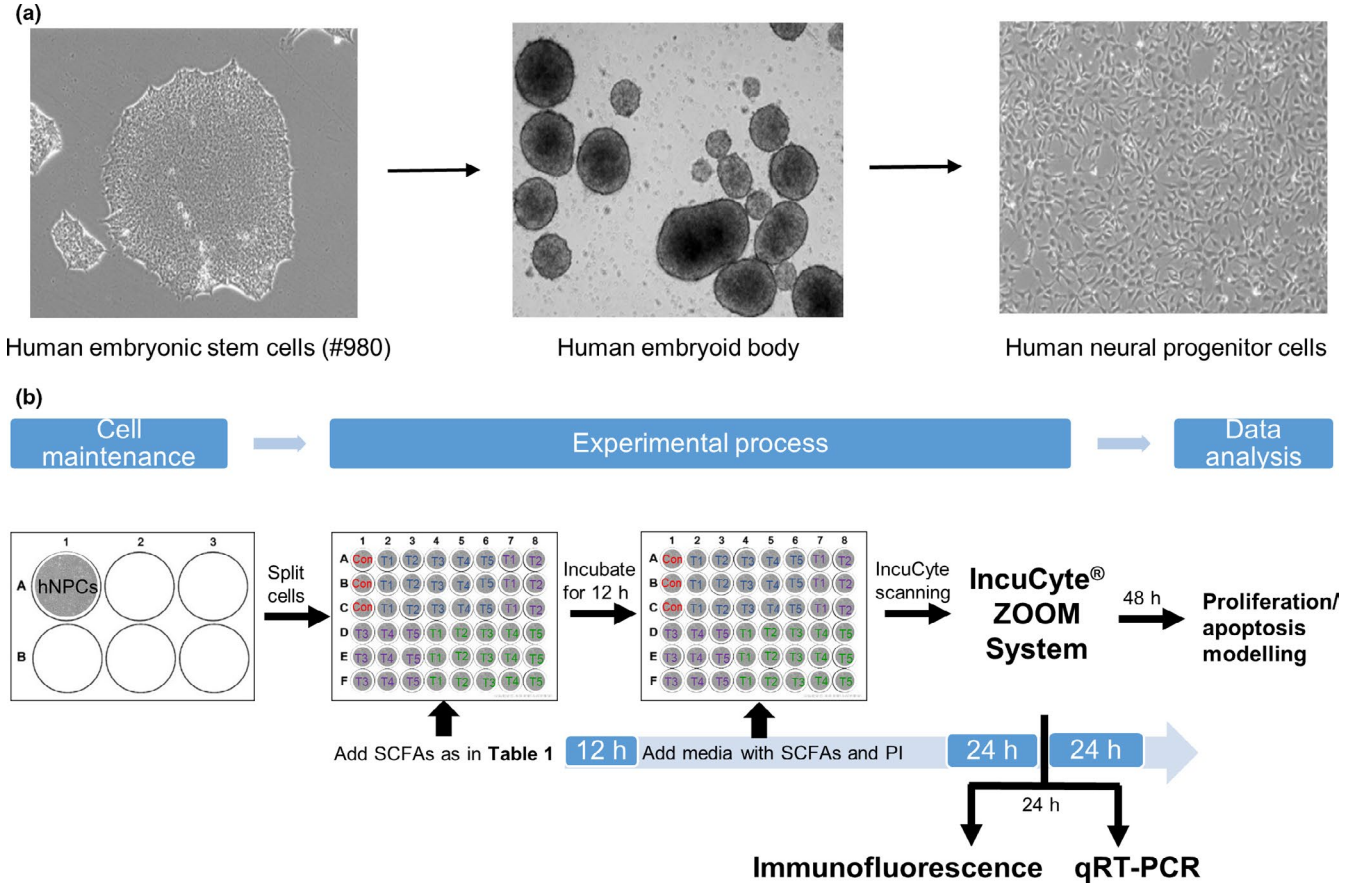

FIGURE 1 Work flow for the generation and SCFA exposure of human neural progenitor cells (hNPCs). (a) Human embryonic stem cell line (HS980) was cultured to get the floating aggregates, human embryoid bodies. Neural rosettes were picked up and cultured for the generation of hNPCs. (b) hNPCs were maintained in a six-well plate, and were then split into a 48-well plate for exposures. Each SCFA treatment condition was in triplicates within one plate and water was used as control. The 48-well plate was incubated for 12 h. Thereafter, 300 µl fresh cell culture media with the same SCFA treatments and propidium iodide (PI) were added and the plate was placed into the IncuCyte. Cells were incubated in the IncuCyte for 48 h for proliferation/apoptosis analyses and for 24 h for immunofluorescence and q-RT PCR analyses

TABLE 1 SCFA concentrations used in this study

(A)	SCFAs	T1	T2	T3	T4	T5
Toxicity test	Acetate	30 µM	3 mM	12 mM	48 mM	192 mM
	Propionate	2 µM	200 µM	800 µM	3.2 mM	12.8 mM
	Butyrate	1 µM	100 µM	400 µM	1.6 mM	6.4 mM
(B)	**SCFAs**	**1**	**2**	**3**	**4**	
Experimental test with physiologically relevant concentrations	Acetate	3 µM	30 µM	300 µM	3 mM	
	Propionate	0.2 µM	2 µM	20 µM	200 µM	
	Butyrate	0.1 µM	1 µM	10 µM	100 µM	

2.4 | LIVE IMAGING USING INCUCYTE® ZOOM SYSTEM

Cells were seeded into 48-well plates and treated in triplicates with SCFAs (sodium acetate, sodium propionate, sodium butyrate or water as control, Table 1) and incubated for 12 hr. Thereafter, 300 µl of fresh medium supplemented with growth factors (EGF, FGF2, N2, B27), SCFAs and 20 µg/ml propidium iodide (PI, cat. #P3566, Invitrogen, Carlsbad, CA, USA) were added into each well and the plate was transferred to the IncuCyte ZOOM system incubator (Essen BioScience) (Figure 1b). PI is a popular red-fluorescent nuclear counterstain, which is not permeant to live cells and commonly used to detect dead cells in a population. Four images were taken from each well every second hour and the confluency percentage data and red

staining count were recorded at the same time. Apoptosis rate was calculated as change in number of dead cells over two hours, and the value reported per condition and plate (one biological experiment) was the mean of the triplicates' mean of the four images per well.

2.5 | MODELING CELL GROWTH

Confluency was assessed at four separate places in each well every second hour. In order to model the sigmoid growth curve, a nonlinear least square model was fitted to the data by finding the best coefficients: $Confluency = phi1 + \frac{phi4 - phi1}{1 + e^{-(phi2 + phi3 \times Time)}}$, where *phi*1 is the confluency at origin, *phi*4 the confluency reached at maximum and -*phi*2/*phi*3 the time corresponding to the inflection point of the curve. Using the estimates of the coefficients and the function's derivative, the maximum growth for each image was calculated (Figure S2). The mean values of maximum growth rate per well in each plate were then calculated. The mean maximum growth rates of each condition from each plate (i.e., mean of the triplicates) were then used for statistical analyses. Seven biological experiments were performed.

2.6 | IMMUNOFLUORESCENCE FOR PHOSPHO-HISTONE H3 (pHH3)

Cells were assessed for expression of pHH3, a marker of mitosis (Kim et al., 2017; Veras, Malpica, Deavers, & Silva, 2009). A plate design identical to that used for assessing maximum growth rate and apoptosis rate was applied. After being treated with SCFAs for 24 h, cells were washed twice with phosphate-buffered saline (PBS, cat. #10010056, Gibco) and fixed with 4% formaldehyde (cat. #R37814, Invitrogen) on ice for 30 min. Cells were washed twice more with PBT buffer (PBS + 0.5% Tween-20 (cat. #P1379, Sigma-Aldrich)) and blocked with PBTA buffer (PBS + 0.3% TritonX-100 (cat. #T8787, Sigma-Aldrich) + 0.1% bovine serum albumin (cat. #A9647, Sigma-Aldrich) + 5% donkey serum (RRID: AB_2337258, cat. #017000121, Jackson ImmunoResearch Labs, Cambridge, UK)) at 22°C for 40 min. Cells were incubated with pHH3 primary antibody (RRID: AB_304763, cat. #ab5176, Abcam, Cambridge, UK) in PBTA at 4°C overnight, followed by washing twice with PBT and incubating with secondary antibody (RRID: AB_162543, cat. #A31572, Invitrogen) at 22°C for 45 min. After staining with DAPI (RRID: AB_2629482, cat. #D1306, Invitrogen) at 22°C for 5 min, cells were imaged by an automated high-content imaging system--Cell Observer (Zeiss). After loading the layout information of plate and setting parameters of the system, images were taken automatically.

To define intensity threshold corresponding to pHH3 positivity, two pictures were randomly selected from each 48-well plate for analysis. Cell nuclei were defined by ImageJ (bundled with 64-bit Java 1.8.0_112) and the mean intensity of pHH3 staining was measured and classified as positive/negative by a human analyst. A threshold was then set according to the split (Figure S3). Thereafter, automatic cell counting for all images was carried out by ImageJ, which recorded the total number of cells and intensity of the fluorescence of each cell, followed by calculating the percentage of positive cells per well and per condition (each condition in triplicates) corresponding to the pre-defined threshold for each plate by software R (version 3.5.0).

2.7 | GENE SELECTION

By checking the three QIAGEN RT^2 Profiler™ PCR Array panels: Human Neurogenesis, Human Cell Cycle, and Human Apoptosis, candidate genes for the study were selected by applying STRING (https://string-db.org/) analysis, which can generate interaction networks of genes. From the neurogenesis panel, eight genes (adenosine A1 receptor (*ADORA1*), adenosine A2a receptor (*ADORA2A*), BCL2 apoptosis regulator (*BCL2*), E1A-binding protein P300 (*EP300*), histone deacetylase 4 (*HDAC4*), necdin (*NDN*), notch receptor 2 (*NOTCH2*), and vascular endothelial growth factor A (*VEGFA*), who have shown strong confidence of interaction with each other were included in our study (Figure S4a). From each of the cell cycle and apoptosis panels, five commonly studied genes from different clusters, which have strong confidence of interaction to other genes were included (Figure S4b and c). The five cell-cycle genes were serine/threonine kinase (*ATR*), cyclin-dependent kinase 1 (*CDK1*), *CDK2*, cyclin D2 (*CCND2*), E2F transcription factor 1 (*E2F1*), the five apoptosis genes were BH3-interacting domain death agonist (*BID*), caspase 8 (*CASP8*), *CASP3*, fas cell surface death receptor (*FAS*), and tumor protein P53 (*TP53*). In total, 18 genes were analyzed by quantitative reverse transcriptase (qRT)-PCR in six independent cell culture preparations (biological replicas). A molecular interaction network of these 18 candidate genes was generated using STRING, which revealed multiple regulations among these genes.

2.8 | QRT-PCR

hNPCs exposed to the each treatment in three 48-well plates (technical replicates) for 24 h were harvested, respectively, in Trizol Reagent (cat. #15596018, Invitrogen) and then total cellular RNA was extracted using Direct-zol™ RNA MinpRrep Plus Kit (cat. #R2072, Zymo Research) according to the standard manufacturer's instructions and protocols. RNA concentration and purity (A260/A280) were measure by NanoDrop™ 2000 Spectrophotometers (cat. # ND-2000), with concentration at 50 ~ 120 ng/l and A260/A280 at 1.8 ~ 2.1 for all samples. cDNA was synthesized directly after RNA extraction using SuperScript® III First-Strand Synthesis System for qRT-PCR (cat. #18080051, Invitrogen) according to the standard protocol for cDNA synthesis with Veriti™ 96-Well Thermal Cycler (cat. #4375786, Applied Biosystems). qRT-PCR was carried out in a QuantStudio™ 6 Flex Real-Time PCR system (cat. #ZG21SCQSTUDIO6FLEX, Applied Biosystems) using SYBR Green kit (cat. #4368702, Applied Biosystems) following the standard settings. The working system for each reaction was the same (5 µl SYBR

TABLE 2 Primer sequences for mRNA

Genes	Primers
Necdin (*NDN*)	Forward 5' ACCCTAACTTTGCAGCCGAG 3'
	Reverse 5' CTTGACCAGCACGTACCACA 3'
E2F transcription factor 1 (*E2F1*)	Forward 5' CAGCTCATTGCCAAGAAGTCC 3'
	Reverse 5' GCAATGCTACGAAGGTCCTGA 3'
Serine/threonine kinase (*ATR*)	Forward 5' AAAGTTGACCACATTTGCCGC 3'
	Reverse 5' CTGCAGGGCCCAGTTGTAA 3'
Caspase 8 (*CASP8*)	Forward 5' GTGAGCAGATCAGAATTGAGGT 3'
	Reverse 5' CAGGCTCTTGTTGATTTGGGC 3'
BH3 interacting domain death agonist (*BID*)	Forward 5' CGGAATATTGCCAGGCACC 3'
	Reverse 5' AAGACATCACGGAGCAAGGAC 3'
Cyclin-dependent kinase 2 (*CDK2*)	Forward 5' GGCATTCCTCTTCCCCTCATC 3'
	Reverse 5' ACGAACAGGGACTCCAAAAGC 3'
BCL2 apoptosis regulator (*BCL2*)	Forward 5' TCATGTGTGTGGAGAGCGTC 3'
	Reverse 5' TCACTTGTGGCCCAGATAGG 3'
Vascular endothelial growth factor A (*VEGFA*)	Forward 5' ATCCAATCGAGACCCTGGTG 3'
	Reverse 5' GCCTTGGTGAGGTTTGATCC 3'
Fas cell surface death receptor (*FAS*)	Forward 5' AACTTGGAAGGCCTGCATCA 3'
	Reverse 5' GGGTCCGGGTGCAGTTTATT 3'
β-actin (*ACTB*)	Forward 5' AGGAATCCTTCTGACCCATGC 3'
	Reverse 5' CTCACCATGGATGATGATATCGC 3'
Glyceraldehyde−3-phosphate dehydrogenase (*GAPDH*)	Forward 5' CCTGCACCACCAACTGCTTA 3'
	Reverse 5' CCAGTGAGCTTCCCGTTCAG 3'

green, 1 µl 10 µM primer pair, 4 µl cDNA). The specific primer pair sequences (Invitrogen) for mRNA are given in Table 2 and Table S1. The success rate was 100% for all genes. The cycle threshold values for the reference genes were 18 ~ 20, and for the target genes 22 ~ 31. All reactions were run in triplicates and the reference genes for normalization were β-actin (*ACTB*) and glyceraldehyde-3-phosphate dehydrogenase (*GAPDH*). Levels of target mRNA relative to that of the reference genes were calculated applying the $2^{-\Delta\Delta Ct}$ method with the average Ct value of the triplicates and using the control group as the calibrator with QuantStudio Software for 6 Flex (V1.3). Analyses were performed on three independent cell culture preparations with all SCFA concentrations in Table 1B, and three additional independent cell culture preparations with the two lowest SCFA concentrations (Table 1B). Target mRNA levels were similar between normalizing using a single reference gene (*ACTB*) and multi-reference genes (*ACTB* and *GAPDH*) (Fig S5a and b).

2.9 | Statistical analysis

The primary endpoints were maximum growth rate, apoptosis rate and proportion of pHH3 positive cells, while the secondary endpoint was gene expression. All data presented represent the mean of at least three replicates of independent cell culture preparations. Normality of distributions was assessed using Shapiro–Wilk test. Between-group (control vs. treatment) differences of each SCFA (acetate, butyrate, and propionate) were tested using unpaired *t*-tests and *p*-values were adjusted for multiple testing with the Holm–Bonferroni method. All statistical tests were performed using software R (version 3.5.0). An adjusted *p*-value less than 0.05 was considered statistically significant. Neither blinding, assessment of the normality of data distribution, nor test for outliers was performed.

3 | RESULTS

3.1 | Toxicity test of SCFAs on hNPCs

To explore the effects of SCFAs on growth rate in our in vitro hNPC model, we first aimed to assure absence of apparent toxicity of SCFAs at concentrations up to approximately 10 times higher than reported physiological levels in human body fluid (Human Metabolome Database). We conducted a toxicity test of the three SCFAs in the hNPC line using the IncuCyte® ZOOM System. Cells were observed by live imaging over a 48 h incubation with the three individual SCFAs each at five different concentrations (Table 1A). We found that for all the three SCFAs, the highest concentration (T5: Acetate_192 mM, Butyrate_6.4 mM, Propionate_12.8 mM) had obvious toxic effects on the cells with much slower growth as compared to controls from early hours and a proliferation termination and cell death after 24 h exposure (Figure 2a). Cellular morphology looked abnormal at T5 (Figure S6a). Also, the T4 concentration of butyrate had obvious effects on cell proliferation and morphology (Figure 2a and Figure S6a). The cells exposed to low concentrations (T1-T3) showed a similar proliferation pattern as cells in the control condition (Figure 2a). Apoptosis rates were assessed by measuring PI-stained dead cells. Only images at confluency less than 80% were considered in order to reduce the influence of high confluency on the results. We found that the overall apoptosis rates for all three SCFAs were increased at the T5, as well as at the T4 for butyrate compared to controls, with the apoptosis rates of the highest concentration (T5) being 2–3 times higher than that of the control group. The apoptosis rates of the SCFA concentrations T1-T3 were at control levels (Figure 2b). When assessing the images in a qualitative way no difference in morphology was apparent in T1-T3 for any three SCFAs (Figure S6a). Taken together, at least the two lowest concentrations (T1 and T2, covering the reported physiological levels in human body fluid) were without apparent toxic effects on hNPCs for all the three compounds.

3.2 | EFFECTS OF SCFAS AT PHYSIOLOGICALLY RELEVANT LEVELS ON PROLIFERATION AND APOPTOSIS OF HNPCS

In this next step, we analyzed the effects of SCFAs at physiologically relevant concentrations on hNPC proliferation and apoptosis.

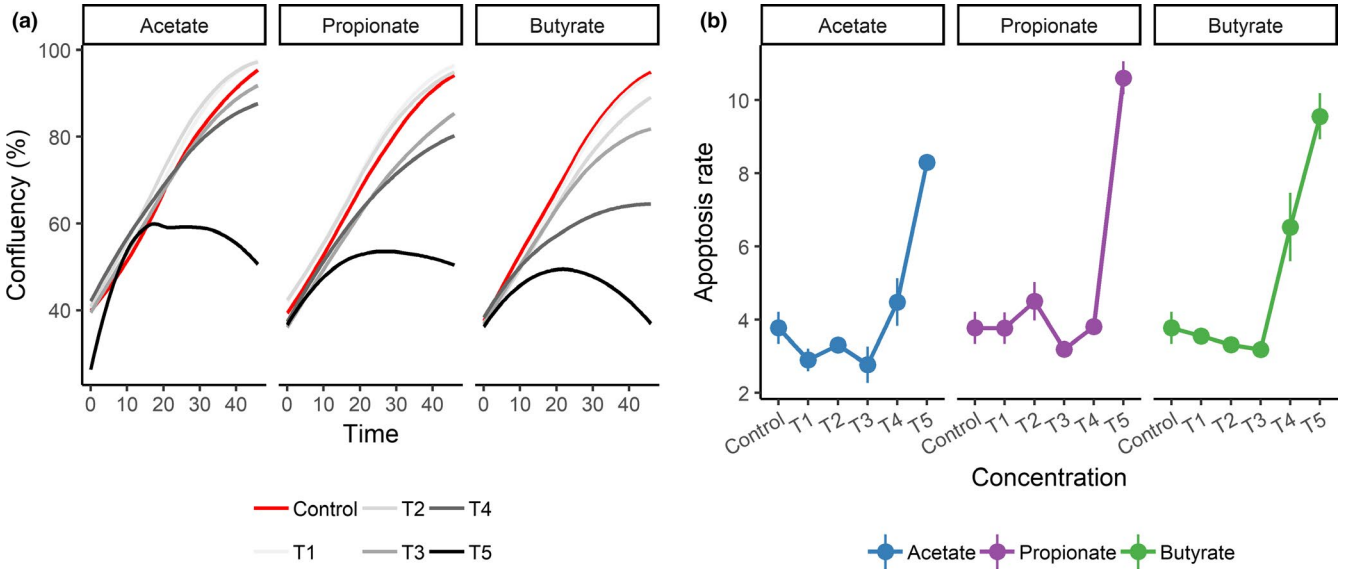

FIGURE 2 Toxicity test of SCFA treatments on human neural progenitor cells (hNPCs). (a) Confluency curve of hNPCs treated with SCFAs over 48 h (concentrations as described in Table 1A). (b) Overall apoptosis rate (Δdead cells/2 h) before reaching 80% confluency during 48 h. Data are presented as mean ± *SEM* and are based on three independent cell culture preparations

Having established that concentrations T1 and T2 of SCFAs were without apparent toxic effects on hNPC, we used concentrations corresponding to T2 and lower of the three compounds (concentrations 1–4, Table 1B). Concentrations 2 and 3 of acetate and all concentrations of butyrate and propionate significantly increased the maximum growth rate of hNSCs, when comparing to the control condition (Figure 3a and Figure S6b). Moreover the three compounds seemed to have a similar dose-dependent effect pattern on maximum growth rate. However, we did not see clear effects of SCFAs on apoptosis rate at any of the confluency stages studied (50%–90% confluency) (Figure 3b and Figure S6b).

To validate these results, we treated the cells for 24 h (Figure 1b), corresponding to the time at which the maximum proliferation was reached, and then stained for phospho-histone H3 (pHH3), a marker of mitosis (Figure 3c), and calculated the proportion of pHH3 positive cells as a proxy-marker for cell proliferation (Figure S3). Acetate concentrations 1 and 3, and propionate concentration 3 (Table 1B), significantly increased the proportion of pHH3 positive cells (Figure 3d), while the highest concentration of the three compounds did not have a significant effect on the proportion of pHH3 positive cells compared to the control (Figure 3d). The dose-dependent effect patterns of the three compounds on proportion of pHH3-positive cells were similar to that on maximum growth rate. Therefore, the three individual SCFAs at physiological levels increased the proliferation rate of hNPCs.

3.3 | GENE EXPRESSION OF HNPCS AFTER TREATMENT WITH SCFAS

To explore molecular mechanisms by which SCFAs mediate proliferation of hNPCs, we selected candidate genes from the three QIAGEN RT^2 Profiler™ PCR Array panels: Human Neurogenesis, Human Cell Cycle and Human Apoptosis. Eight genes (*EP300*, *HDAC4*, *NOTCH2*, *BCL2*, *VEGFA*, *NDN*, *ADORA2A*, *ADORA1*) from the neurogenesis panel, five genes (*CDK1*, *CDK2*, *CCND2*, *ATR*, *E2F1*) from the cell cycle panel and five genes (*CASP3*, *CASP8*, *FAS*, *BID*, *TP53*) from the apoptosis panel were selected. These 18 genes were analysed by qRT-PCR after exposure to all exposure levels (Table 1B) in three independent cell culture preparations (Figure S5a and b). When we combined all data from six independent cell culture preparations with physiologically relevant level of treatments, nine out of 18 genes showed significant changes in expression by SCFA exposure conditions compared to control exposure (Figure 4a). The neurogenesis related gene *ATR*, *NDN*, proliferation related genes *CDK2*, *E2F1*, *VEGFA*, and the apoptosis-related genes *BCL2*, *BID*, *CASP8*, and *FAS* (Figure 4a) were significantly changed in cells treated with SCFAs for 24 h. The expression of the other nine studied genes (*ADORA1*, *ADORA2A*, *CASP3*, *CDK1*, *CCND2*, *EP300*, *NOTCH2*, *HDAC4*, *TP53*) did not change significantly by the SCFAs treatment (data not shown). A molecular interaction network of these 18 candidate genes was generated using STRING (https://string-db.org/). The 18 genes clustered as four groups using the Markov Cluster algorithm, which were discriminated in agreement with the original panels (Figure 4b). The nine genes (*ATR*, *BCL2*, *BID*, *CASP8*, *CDK2*, *E2F1*, *FAS*, *NDN*, *VEGFA*) that showed significant changes after SCFA treatments in our cell model were located in the center of the interaction network and had multiple experimentally validated molecular actions, which may suggest possible pathways among these genes (Figure 4b).

4 | DISCUSSION

We show for the first time by two separate analysis methods that the SCFAs acetate, propionate and butyrate promote proliferation

of hNPCs at physiologically relevant concentrations (e.g., CSF: acetate 31–410 μM, propionate 0–6 μM, butyrate 0–2.8 μM, Human Metabolome Database). Furthermore, we could not detect any effect on hNPC apoptosis at these levels. The strongest effects were found in the levels close to CSF (concentrations 2 and 3 in Table 1B). These findings were supported by that several genes,

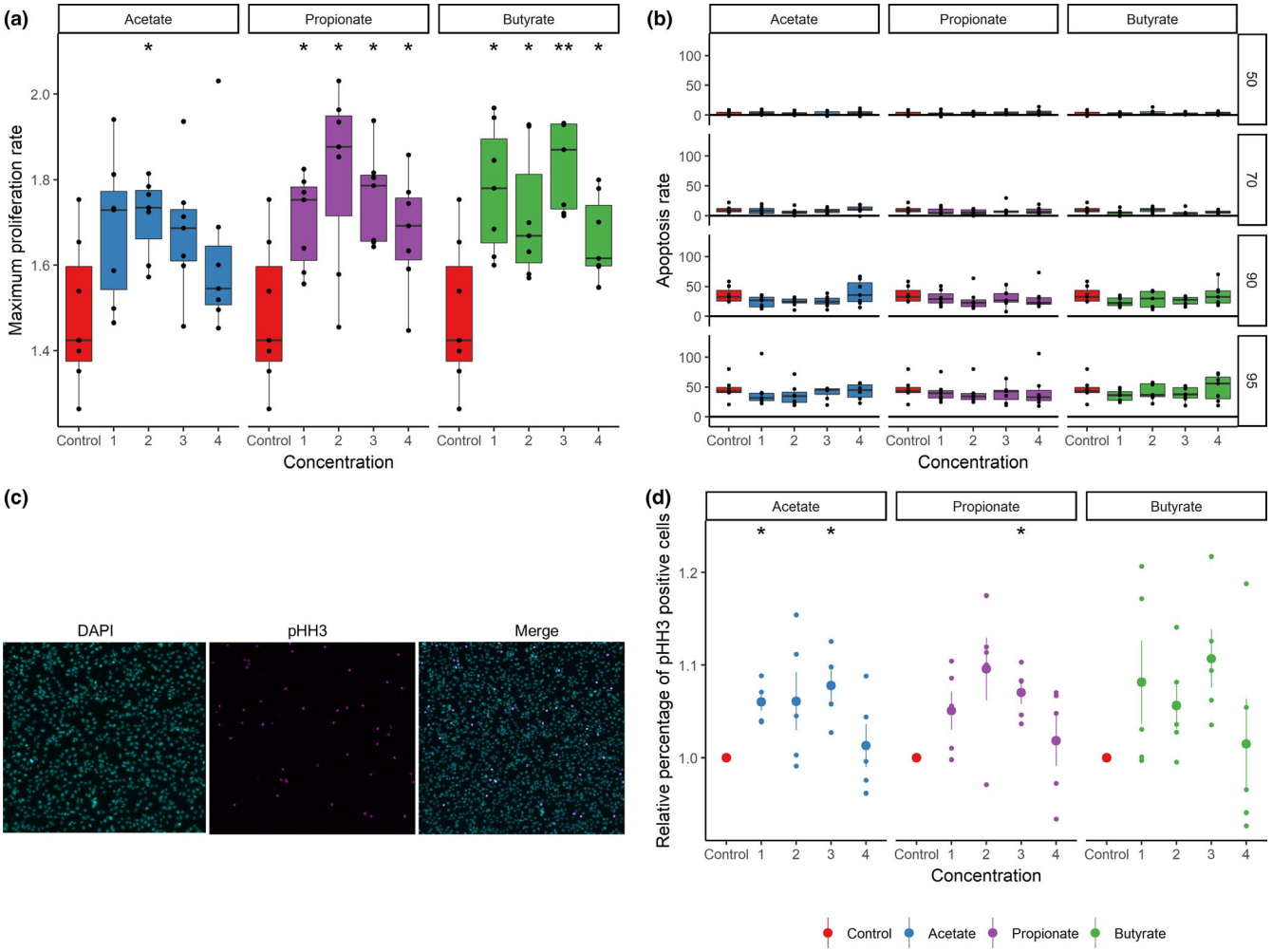

FIGURE 3 Proliferation and apoptosis effects of SCFA treatments on human neural progenitor cells (hNPCs). (a). Maximum proliferation rate estimated from the growth curves for all treatments (n = 7) monitored using IncuCyte live imaging. (b). Apoptosis rate (Δdead cells/2 h) based on propidium iodide (PI) staining for different treatments at different confluency stages (50%–95%) (n = 7) monitored using IncuCyte live imaging. Box represents the interquartile range (IQR), line inside box represents median, lower and upper whisker indicate 1st quartile (Q1) minus 1.5 × IQR and Q3 plus 1.5 × IQR. (c). Phospho histone H3 (pHH3) and nuclear (DAPI) staining of hNPCs after treating with three SCFAs for 24 h. (d). pHH3 positive cell percentage for each group (n = 5), all groups were normalized with the ratio of control group (red), making control group to 1.0. Data here are presented as mean ± *SEM*, acetate (blue), butyrate (green), propionate (purple). All between-group differences within each SCFA were compared with by unpaired t-tests comparing each treatment group to control followed by Holm–Bonferroni correction. * adjusted p value < 0.05, ** adjusted p < .01. n refers to number of independent cell culture preparations (48-well plate)

FIGURE 4 Genes known to be involved in proliferation and/or apoptosis had altered expression levels in human neural progenitor cells (hNPCs) after exposure to physiologically relevant levels of SCFAs. (a). Cells treated with physiologically relevant levels (Table 1B) of a SCFAs (acetate, butyrate, and propionate) for 24 h were assessed for gene expression of 18 genes known to be implicated in neurogenesis, cell cycle, or apoptosis using qRT-PCR. Nine of the analyzed genes had altered levels after at least one SCFA concentration exposure. The number of independent cell culture preparations was 6 for the lower concentration groups 1 and 2, and 3 for the higher concentration groups 3 and 4. (b). Molecular interaction network for the 18 genes using STRING with basic settings: Network edges (molecular action), Experiments (active interaction sources), Markov cluster algorithm (algorithm). Shape and color of the lines between the genes indicate the predicted mode of action, and the gene colors indicate gene clusters. The nine genes in figure (a) are indicated with † in (b). The bars represent the mean ± *SEM*. The controls (red) within each plate were used as and set to 1.0. Between-group (control vs. treatment) differences of each SCFA (acetate, butyrate and propionate) were tested using unpaired t-tests and p-values were adjusted for multiple testing with the Holm–Bonferroni method. *adjusted p < .05, **adjusted p < .01

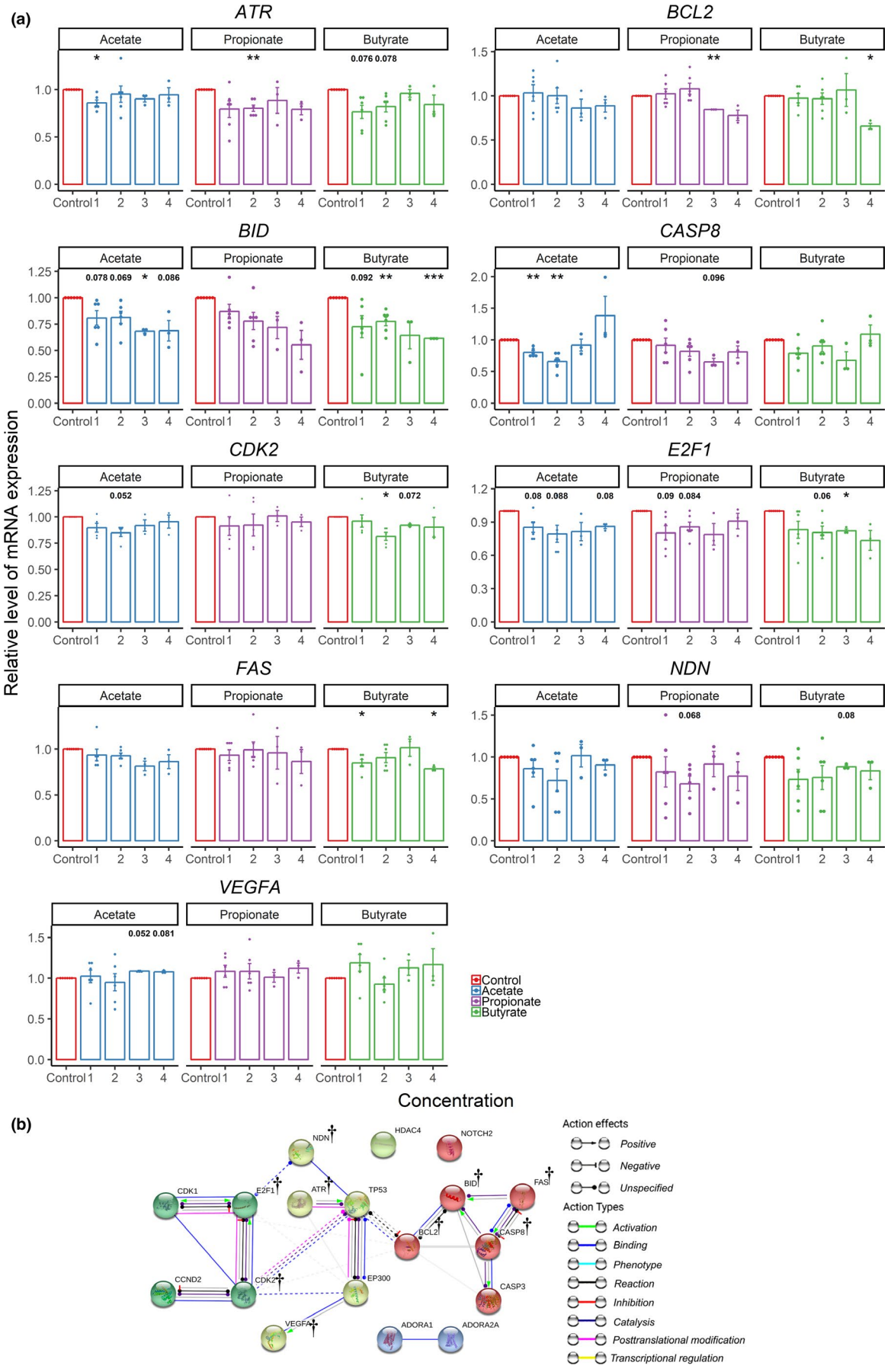
(a)
ATR
BCL2
BID
CASP8
CDK2
E2F1
FAS
NDN
VEGFA
Acetate
Propionate
Butyrate
Relative level of mRNA expression
Control
Acetate
Propionate
Butyrate
Concentration
(b)
NDN
HDAC4
NOTCH2
CDK1
E2F1
ATR
TP53
BID
FAS
BCL2
CASP8
CCND2
CDK2
EP300
CASP3
VEGFA
ADORA1
ADORA2A
Action effects
Positive
Negative
Unspecified
Action Types
Activation
Binding
Phenotype
Reaction
Inhibition
Catalysis
Posttranslational modification
Transcriptional regulation

previously reported to be involved in neurogenesis, proliferation, and apoptosis, showed significant expression changes by the corresponding SCFA exposures. This finding is consistent with another recent study showing that propionate increased diameter of neurospheres from hNSCs (Abdelli, Samsam, & Naser, 2019). Toxic effects were found only at much higher concentration, in agreement with studies of high dose propionate infusions in rat brain where we did not observe increased apoptosis in brain despite the presence of autism spectrum disorder-like behaviors, seizure, neuroinflammation, and redox changes (MacFabe et al., 2007).

The SCFAs present in the human body fluid derive mainly from bacterial carbohydrate fermentation in the gut. However, they are also present naturally in dairy, fermented foods, maternal milk and are added as antifungal agents in refined carbohydrates and dairy. The amounts and composition of gut short-chain fatty acids are dependent not only on bacterial species but also on type of substrate (increased propionate with wheat and dairy, increased butyrate with inulin-containing diets). Their effects are remarkably tissue and dose specific (Al-Lahham, Peppelenbosch, Roelofsen, Vonk, & Venema, 2010; MacFabe, 2015). Studies on animal models and cell lines have shown that SCFAs influence diverse processes in nervous system physiology and behaviors, and orally administered SCFAs can cause such effects as well (see introduction). ^{13}C-labelled acetate derived from dietary carbohydrates was observed to cross the BBB, reach the rat brain and regulate appetite (Frost, Sleeth, & Sahuri-Arisoylu, 2014). In germ-free mice that exhibited an impairment of the BBB and microglial function, SCFAs in drinking water restored these functions (Braniste et al., 2014; Erny et al., 2015). Moreover maternal SCFAs have been reported to influence the fetus, as subcutaneous injection of propionate into pregnant dams increased the anxious behavior in the female rat offspring (Foley et al., 2014).

To the best of our knowledge, there are few in vitro studies of SCFA effects on hNPCs published so far. The vast majority of previous in vitro studies of SCFA effects were performed on cancer cells (see introduction). Also, the concentrations of SCFAs applied in these studies were at mM range, acetate (1–26 mM), butyrate (0.1–20 mM), and propionate (1–10 mM), which were mostly much higher than physiological levels in human blood, urine, and CSF. The study most comparable to ours was conducted with 2 mM propionate on hNSCs, which showed effects of increasing diameter of neurospheres (Abdelli et al., 2019). In order to model physiology in this study, we used SCFA concentrations in a µM to mM range, with proportions of acetate: butyrate: propionate proportions at about 30:1:2 (Table 1), similar to the levels observed in blood (Cummings et al., 1987; Hoyles et al., 2018; Peters, Pomare, & Fisher, 1992), urine (Zhao et al., 2017) and CSF (Nagashima et al., 2010; Pal, Sharma, Gupta, Pratap, & Jagannathan, 2005). Our results indicated that all three SCFAs at µM levels had proliferative effects on hNPCs. Accordingly, a newly published in vitro study showed a protective effect on a human BBB model of propionate exposure at 1 µM for 24 h and that 10–100 times higher propionate levels did not compromise these protective effects (Hoyles et al., 2018).

SCFAs can exert effects through several mechanisms. First, they activate the G-protein-coupled receptors primarily GPR41/FFAR3 and GPR43/FFAR2. Both receptors were expressed in the hNPCs studied here and were potentially up-regulated by SCFA exposure (Figure S7). Second, due to their carboxylic group they may influence the pH, affecting many processes including gap junction closure, leading to electrotonic, neurodevelopmental and anti-apoptotic effects (Frantseva et al., 2002; MacFabe, 2015). Thirdly, they have epigenetic effects through their HDAC inhibitory activity on regulating gene expression (Kim et al., 2009; MacFabe, 2015; Patnala, Arumugam, Gupta, & Dheen, 2016; Yao et al., 2010). In our study, several genes involved in neurogenesis, proliferation and apoptosis were significantly down-regulated by the SCFAs. These effects might not be mediated through HDAC inhibition, as that mostly is associated with transcription activation. Effects via mitochondrial induced pathways may possibly be involved (Frye et al., 2017).

Strengths of our study are particularly the human origin of the NPCs, that we explored effects of physiologically relevant concentrations of the three most common SCFAs, the live imaging in combination with a mitosis marker and finally the relatively high number of biological replicas. Limitations of the study include that it is based on an in vitro 2D-model and that it lacks data from exposure to combinations of SCFAs.

5 | CONCLUSION

Our study demonstrates, for the first time, that SCFAs, at human physiological concentrations, increase the proliferation and mitosis of human early neural progenitor cells. These findings have implications for further evidence of maternal gut microbiota influence on fetal brain development, a putative 'maternal gut-fetal brain-axis', and further support the role of dietary and enteric short-chain fatty acid and associated pathways in brain development and function, in both health and disease.

ACKNOWLEDGMENTS

This study was financially supported by the Swedish Research Council (CL), the Swedish Brain Foundation (CL) and the China Scholarship Council (www.scs.edu.cn, LY). L.L.Y., C.L., D.F.M., and J.C.V. designed the study. S.R. provided the hNPCs. L.L.Y. performed all the assays in this study. V.M. performed the modeling of cell proliferation. L.L.Y. and V.M. undertook the statistical analyses. L.L.Y. wrote draft of the manuscript and all the other authors interpreted the results and revised the manuscript. All authors read and approved the final manuscript.

CONFLICT OF INTEREST

The authors declare no conflicts of interest relevant to this article. All experiments were conducted in compliance with the ARRIVE guidelines.

DATA AVAILABILITY STATEMENT

The data that support the findings of this study are available from the corresponding author upon reasonable request.

ORCID

Liu L. Yang https://orcid.org/0000-0002-5963-6295
Vincent Millischer https://orcid.org/0000-0003-1919-9649

REFERENCES

Aagaard, K., Ma, J., Antony, K. M., Ganu, R., Petrosino, J., & Versalovic, J. (2014). The placenta harbors a unique microbiome. *Science Translational Medicine*, *6*, 237ra265.

Abdelli, L. S., Samsam, A., & Naser, S. A. (2019). Propionic acid induces gliosis and Neuro-inflammation through Modulation of PTEN/AKT Pathway in Autism Spectrum Disorder. *Scientific Reports*, *9*, 8824.

Al-Lahham, S. H., Peppelenbosch, M. P., Roelofsen, H., Vonk, R. J., & Venema, K. (2010). Biological effects of propionic acid in humans; metabolism, potential applications and underlying mechanisms. *Biochimica Et Biophysica Acta*, *1801*, 1175–1183.

Ardissone, A. N., de la Cruz, D. M., Davis-Richardson, A. G. *et al.* (2014). Meconium microbiome analysis identifies bacteria correlated with premature birth. *PLoS ONE*, *9*, e90784.

Bienenstock, J., Kunze, W., & Forsythe, P. (2015). Microbiota and the gut-brain axis. *Nutrition Reviews*, *73*(Suppl 1), 28–31.

Braniste, V., Al-Asmakh, M., Kowal, C. *et al.* (2014). The gut microbiota influences blood-brain barrier permeability in mice. *Science Translational Medicine*, *6*, 263ra158.

Buffington, S. A., Di Prisco, G. V., Auchtung, T. A., Ajami, N. J., Petrosino, J. F., & Costa-Mattioli, M. (2016). Microbial reconstitution reverses maternal diet-induced social and synaptic deficits in offspring. *Cell*, *165*, 1762–1775.

Cummings, J. H., Pomare, E. W., Branch, W. J., Naylor, C. P., & Macfarlane, G. T. (1987). Short chain fatty acids in human large intestine, portal, hepatic and venous blood. *Gut*, *28*, 1221–1227.

De Baere, S., Eeckhaut, V., Steppe, M., De Maesschalck, C., De Backer, P., Van Immerseel, F., & Croubels, S. (2013). Development of a HPLC-UV method for the quantitative determination of four short-chain fatty acids and lactic acid produced by intestinal bacteria during in vitro fermentation. *Journal of Pharmaceutical and Biomedical Analysis*, *80*, 107–115.

DeCastro, M., Nankova, B. B., Shah, P., Patel, P., Mally, P. V., Mishra, R., & La Gamma, E. F. (2005). Short chain fatty acids regulate tyrosine hydroxylase gene expression through a cAMP-dependent signaling pathway. *Brain Research. Molecular Brain Research*, *142*, 28–38.

Diaz Heijtz, R., Wang, S., Anuar, F., Qian, Y., Bjorkholm, B., Samuelsson, A., … Pettersson, S. (2011). Normal gut microbiota modulates brain development and behavior. *Proceedings of the National Academy of Sciences of the United States of America*, *108*, 3047–3052.

Dinan, T. G., & Cryan, J. F. (2017). Brain-gut-microbiota axis and mental health. *Psychosomatic Medicine*, *79*, 920–926.

Erny, D., Hrabe de Angelis, A. L., Jaitin, D. *et al.* (2015). Host microbiota constantly control maturation and function of microglia in the CNS. *Nature Neuroscience*, *18*, 965–977.

Falk, A., Koch, P., Kesavan, J. *et al.* (2012). Capture of neuroepithelial-like stem cells from pluripotent stem cells provides a versatile system for in vitro production of human neurons. *PLoS ONE*, *7*, e29597.

Foley, K. A., Ossenkopp, K. P., Kavaliers, M., & Macfabe, D. F. (2014). Pre- and neonatal exposure to lipopolysaccharide or the enteric metabolite, propionic acid, alters development and behavior in adolescent rats in a sexually dimorphic manner. *PLoS ONE*, *9*, e87072.

Frantseva, M. V., Kokarovtseva, L., Naus, C. G., Carlen, P. L., MacFabe, D., & Perez Velazquez, J. L. (2002). Specific gap junctions enhance the neuronal vulnerability to brain traumatic injury. *Journal of Neuroscience*, *22*, 644–653.

Frost, G., Sleeth, M. L., Sahuri-Arisoylu, M. *et al.* (2014). The short-chain fatty acid acetate reduces appetite via a central homeostatic mechanism. *Nature Communications*, *5*, 3611.

Frye, R. E., Melnyk, S., & Macfabe, D. F. (2013). Unique acyl-carnitine profiles are potential biomarkers for acquired mitochondrial disease in autism spectrum disorder. *Translational Psychiatry*, *3*, e220.

Frye, R. E., Nankova, B., Bhattacharyya, S., Rose, S., Bennuri, S. C., & MacFabe, D. F. (2017). Modulation of immunological pathways in autistic and Neurotypical Lymphoblastoid cell lines by the enteric microbiome metabolite propionic acid. *Frontiers in Immunology*, *8*, 1670.

Hecker, M., Sommer, N., Voigtmann, H. *et al.* (2014). Impact of short- and medium-chain fatty acids on mitochondrial function in severe inflammation. JPEN. *Journal of Parenteral and Enteral Nutrition*, *38*, 587–594.

Hoyles, L., Snelling, T., Umlai, U. K., Nicholson, J. K., Carding, S. R., Glen, R. C., & McArthur, S. (2018). Microbiome-host systems interactions: Protective effects of propionate upon the blood-brain barrier. *Microbiome*, *6*, 55.

Hsiao, E. Y., McBride, S. W., Hsien, S. *et al.* (2013). Microbiota modulate behavioral and physiological abnormalities associated with neurodevelopmental disorders. *Cell*, *155*, 1451–1463.

Hu, J., Kyrou, I., Tan, B. K. *et al.* (2016). Short-chain fatty acid acetate stimulates adipogenesis and mitochondrial biogenesis via GPR43 in brown adipocytes. *Endocrinology*, *157*, 1881–1894.

Hu, J., Lin, S., Zheng, B., & Cheung, P. C. K. (2018). Short-chain fatty acids in control of energy metabolism. *Critical Reviews in Food Science and Nutrition*, *58*, 1243–1249.

Jimenez, E., Fernandez, L., Marin, M. L. *et al.* (2005). Isolation of commensal bacteria from umbilical cord blood of healthy neonates born by cesarean section. *Current Microbiology*, *51*, 270–274.

Jin, X., Wu, N., Dai, J., Li, Q., & Xiao, X. (2017). TXNIP mediates the differential responses of A549 cells to sodium butyrate and sodium 4-phenylbutyrate treatment. *Cancer Medicine*, *6*, 424–438.

Kasubuchi, M., Hasegawa, S., Hiramatsu, T., Ichimura, A., & Kimura, I. (2015). Dietary gut microbial metabolites, short-chain fatty acids, and host metabolic regulation. *Nutrients*, *7*, 2839–2849.

Kelly, J. R., Borre, Y., C, O. B., *et al.* (2016). Transferring the blues: Depression-associated gut microbiota induces neurobehavioural changes in the rat. *Journal of Psychiatric Research*, *82*, 109–118.

Kim, H. J., Leeds, P., & Chuang, D.-M. (2009). The HDAC inhibitor, sodium butyrate, stimulates neurogenesis in the ischemic brain. *Journal of Neurochemistry*, *110*, 1226–1240.

Kim, J. Y., Jeong, H. S., Chung, T., Kim, M., Lee, J. H., Jung, W. H., & Koo, J. S. (2017). The value of phosphohistone H3 as a proliferation marker for evaluating invasive breast cancers: A comparative study with Ki67. *Oncotarget*, *8*, 65064–65076.

Koch, P., Opitz, T., Steinbeck, J. A., Ladewig, J., & Brustle, O. (2009). A rosette-type, self-renewing human ES cell-derived neural stem cell with potential for in vitro instruction and synaptic integration. *Proceedings of the National Academy of Sciences of the United States of America*, *106*, 3225–3230.

Levenson, J. M., O'Riordan, K. J., Brown, K. D., Trinh, M. A., Molfese, D. L., & Sweatt, J. D. (2004). Regulation of histone acetylation during memory formation in the hippocampus. *The Journal of Biological Chemistry*, *279*, 40545–40559.

Lin, Y., Fang, Z. F., Che, L. Q., Xu, S. Y., Wu, D., Wu, C. M., & Wu, X. Q. (2014). Use of sodium butyrate as an alternative to dietary fiber: Effects on the embryonic development and anti-oxidative capacity of rats. *PLoS ONE*, *9*, e97838.

Luczynski, P., McVey Neufeld, K.-A., Oriach, C. S., Clarke, G., Dinan, T. G., & Cryan, J. F. (2016) Growing up in a bubble: Using germ-free animals to assess the influence of the gut microbiota on brain and behavior. *The International Journal of Neuropsychopharmacology 19*, pyw020.

MacFabe, D. F. (2015). Enteric short-chain fatty acids: Microbial messengers of metabolism, mitochondria, and mind: Implications in autism spectrum disorders. *Microbial Ecology in Health and Disease*, *26*, 28177.

MacFabe, D. F., Cain, D. P., Rodriguez-Capote, K., Franklin, A. E., Hoffman, J. E., Boon, F., … Ossenkopp, K. P. (2007). Neurobiological effects of intraventricular propionic acid in rats: Possible role of short chain fatty acids on the pathogenesis and characteristics of autism spectrum disorders. *Behavioural Brain Research*, *176*, 149–169.

Miyamoto, J., Hasegawa, S., Kasubuchi, M., Ichimura, A., Nakajima, A., & Kimura, I. (2016). Nutritional signaling via free fatty acid receptors. *International Journal of Molecular Sciences*, *17*, 450.

Nagashima, H., Morio, Y., Meshitsuka, S., Yamane, K., Nanjo, Y., & Teshima, R. (2010). High-resolution nuclear magnetic resonance spectroscopic study of metabolites in the cerebrospinal fluid of patients with cervical myelopathy and lumbar radiculopathy. *European Spine Journal : Official Publication of the European Spine Society, the European Spinal Deformity Society, and the European Section of the Cervical Spine Research Society*, *19*, 1363–1368.

Nankova, B. B., Agarwal, R., MacFabe, D. F., & La Gamma, E. F. (2014). Enteric bacterial metabolites propionic and butyric acid modulate gene expression, including CREB-dependent catecholaminergic neurotransmission, in PC12 cells–possible relevance to autism spectrum disorders. *PLoS ONE*, *9*, e103740.

Ntranos, A., & Casaccia, P. (2018). The Microbiome-Gut-Behavior Axis: Crosstalk Between the Gut Microbiome and Oligodendrocytes Modulates Behavioral Responses. *Neurotherapeutics : The Journal of the American Society for Experimental NeuroTherapeutics*, *15*, 31–35.

Orczyk-Pawilowicz, M., Jawien, E., Deja, S., Hirnle, L., Zabek, A., & Mlynarz, P. (2016). Metabolomics of human amniotic fluid and maternal plasma during normal pregnancy. *PLoS ONE*, *11*, e0152740.

Pal, K., Sharma, U., Gupta, D. K., Pratap, A., & Jagannathan, N. R. (2005). Metabolite profile of cerebrospinal fluid in patients with spina bifida: A proton magnetic resonance spectroscopy study. *Spine*, *30*, E68–72.

Patnala, R., Arumugam, T. V., Gupta, N., & Dheen, S. T. (2016). HDAC inhibitor sodium butyrate-mediated epigenetic regulation enhances neuroprotective function of microglia during ischemic stroke. *Molecular Neurobiology*.

Patnala, R., Arumugam, T. V., Gupta, N., & Dheen, S. T. (2017). HDAC inhibitor sodium butyrate-mediated epigenetic regulation enhances neuroprotective function of microglia during ischemic stroke. *Molecular Neurobiology*, *54*, 6391–6411.

Perego, S., Sansoni, V., Banfi, G., & Lombardi, G. (2018). Sodium butyrate has anti-proliferative, pro-differentiating, and immunomodulatory effects in osteosarcoma cells and counteracts the TNFalpha-induced low-grade inflammation. *International Journal of Immunopathology and Pharmacology*, *32*, 394632017752240.

Peters, S. G., Pomare, E. W., & Fisher, C. A. (1992). Portal and peripheral blood short chain fatty acid concentrations after caecal lactulose instillation at surgery. *Gut*, *33*, 1249–1252.

Rodin, S., Antonsson, L., Niaudet, C. *et al.* (2014). Clonal culturing of human embryonic stem cells on laminin-521/E-cadherin matrix in defined and xeno-free environment. *Nature Communications*, *5*, 3195.

Rorig, B., Klausa, G., & Sutor, B. (1996). Intracellular acidification reduced gap junction coupling between immature rat neocortical pyramidal neurones. *The Journal of Physiology*, *490*(Pt 1), 31–49.

Rose, S., Bennuri, S. C., Davis, J. E. *et al.* (2018). Butyrate enhances mitochondrial function during oxidative stress in cell lines from boys with autism. *Translational Psychiatry*, *8*, 42.

Severson, C. A., Wang, W., Pieribone, V. A., Dohle, C. I., & Richerson, G. B. (2003). Midbrain serotonergic neurons are central pH chemoreceptors. *Nature Neuroscience*, *6*, 1139–1140.

Sharon, G., Cruz, N. J., Kang, D. W., Gandal, M. J., Wang, B., Kim, Y. M., … Mazmanian, S. K. (2019). Human gut microbiota from autism spectrum disorder promote behavioral symptoms in mice. *Cell*, *177*, 1600–1618.e1617.

Sivaprakasam, S., Prasad, P. D., & Singh, N. (2016). Benefits of short-chain fatty acids and their receptors in inflammation and carcinogenesis. *Pharmacology & Therapeutics*, *164*, 144–151.

Stinson, L. F., Boyce, M. C., Payne, M. S., & Keelan, J. A. (2019). The not-so-sterile womb: Evidence that the human fetus is exposed to bacteria prior to birth. *Frontiers in Microbiology*, *10*, 1124.

Tsuji, A. (2005). Small molecular drug transfer across the blood-brain barrier via carrier-mediated transport systems. *NeuroRx: The Journal of the American Society for Experimental NeuroTherapeutics*, *2*, 54–62.

Van Rymenant, E., Abranko, L., Tumova, S., Grootaert, C., Van Camp, J., Williamson, G., & Kerimi, A. (2017). Chronic exposure to short-chain fatty acids modulates transport and metabolism of microbiome-derived phenolics in human intestinal cells. *Journal of Nutritional Biochemistry*, *39*, 156–168.

Veras, E., Malpica, A., Deavers, M. T., & Silva, E. G. (2009). Mitosis-specific marker phospho-histone H3 in the assessment of mitotic index in uterine smooth muscle tumors: A pilot study. *International Journal of Gynecological Pathology : Official Journal of the International Society of Gynecological Pathologists*, *28*, 316–321.

Vijay, N., & Morris, M. E. (2014). Role of monocarboxylate transporters in drug delivery to the brain. *Current Pharmaceutical Design*, *20*, 1487–1498.

Wang, Y., Hu, P. C., Ma, Y. B., Fan, R., Gao, F. F., Zhang, J. W., & Wei, L. (2016). Sodium butyrate-induced apoptosis and ultrastructural changes in MCF-7 breast cancer cells. *Ultrastructural Pathology*, *40*, 200–204.

Wei, Y., Melas, P. A., Wegener, G., Mathe, A. A., & Lavebratt, C. (2014). Antidepressant-like effect of sodium butyrate is associated with an increase in TET1 and in 5-hydroxymethylation levels in the Bdnf gene. *The International Journal of Neuropsychopharmacology*, *18*.

Yao, X., Zhang, J. R., Huang, H. R., Dai, L. C., Liu, Q. J., & Zhang, M. (2010). Histone deacetylase inhibitor promotes differentiation of embryonic stem cells into neural cells in adherent monoculture. *Chinese Medical Journal*, *123*, 734–738.

Yoo, D. Y., Kim, W., Nam, S. M., Kim, D. W., Chung, J. Y., Choi, S. Y., … Hwang, I. K. (2011). Synergistic effects of sodium butyrate, a histone deacetylase inhibitor, on increase of neurogenesis induced by pyridoxine and increase of neural proliferation in the mouse dentate gyrus. *Neurochemical Research*, *36*, 1850–1857.

Zhao, R., Chu, L., Wang, Y., Song, Y., Liu, P., Li, C., … Kang, X. (2017). Application of packed-fiber solid-phase extraction coupled with GC-MS for the determination of short-chain fatty acids in children's urine. *Clinica Chimica Acta*, *468*, 120–125.

Zheng, P., Zeng, B., Liu, M. *et al.* (2019). The gut microbiome from patients with schizophrenia modulates the glutamate-glutamine-GABA cycle and schizophrenia-relevant behaviors in mice. *Science Advances*, *5*, eaau8317.

SUPPORTING INFORMATION

Additional supporting information may be found online in the Supporting Information section.

How to cite this article: Yang LL, Millischer V, Rodin S, MacFabe DF, Villaescusa JC, Lavebratt C. Enteric short-chain fatty acids promote proliferation of human neural progenitor cells. *J. Neurochem.*. 2019;00:e14928. https://doi.org/10.1111/jnc.14928